Experimental Correction of Radiation Patterns Between Electromagnetic Environments

Maxime Spirlet, *Student Member, IEEE,* Christophe Geuzaine, *Member, IEEE* and Véronique Beauvois, *Member, IEEE*

***Abstract*—This manuscript presents an experimental method to estimate a radiation pattern obtained in a particular echoic environment (for example from in-situ measurements) as if measurements were performed in a given anechoic chamber. The correction is achieved using some reference measurements collected both in echoic and anechoic environments. An angular transfer function is estimated from these two sets of measurements and deconvolved from the measured radiation pattern to be corrected.**

***Index Terms*—Pattern deconvolution, angular deconvolution, radiation pattern estimation.**

I. Introduction

ACHIEVING measurements of antenna radiation patterns generally relies on a regulated environment to obtain accurate (precise and true) results [1]–[3]. Being part of this environment, the area where the measurements are performed has a huge impact on the obtained quality and trueness.

The use of anechoic chambers helps delivering high quality levels, compared to undedicated sites. Indeed, the high shielding effectiveness of the metalic enclosure prevents external sources to interfer with the measured source (and conversely). The absorbing materials also prevent undesired reflections to cause spurious patterns by greatly reducing them.

But sometimes, for various reasons, there is no other option than performing in-situ measurements of an antenna or an equipment radiation pattern. Among those reasons, one could cite issues concerning the size or the weight of the antenna or the object to be measured compared to the available anechoic room, or the expensive cost due to the use of such a facility.

Many techniques have been proposed in the literature to correct echoic patterns. Arriving echoes can be treated using compensation methods [4] or more intuitively by considering the time delay approach [5], in which the direct propagation path, without echo is assessed to have the shortest time delay. Using the Discrete Fourier Transform (DFT) on the frequency samples, the direct path is identified and isolated in the time domain, and then transformed back in the frequency domain to recover the anechoic pattern. However, depending on the time delay between the Line Of Sight (LOS) path and the first echo, this method requires important bandwidth, which can not always be met with narrowband antennas. The excessive frequency sampling rate can also cause measurement overhead to obtain accurate results. The Matrix Pencil Method (MPM) [6]–[11] overcomes some of these problems by reducing the required bandwidth. This method decomposes a frequency sequence into a sum of exponentials, from which it is therefore possible to isolate the contribution of the direct path and from the echoes, based on the argument of the exponentials. Compared to the DFT method, this one requires less bandwidth but is much more sensitive to noise in processed data, causing some decrease in the quality of the reconstructed anechoic pattern. And finally, there exists methods based on the sparse deconvolution of a frequency sequence [12], [13]. A statistical method called Maximum A Priori (MAP), using a Cauchy-Gauss model to approximate the frequency response, is applied to regularize the processed sequence while a DFT algorithm is applied. This overcomes the windowing problem of the DFT by reducing the lobes induced in the dual domain, which is highly enhanced when introducing zero fill-in to increase the resolution in the dual domain. A rather similar method, using *a priori* data has also been developed [14], where the frequency response is approximated using Chebyshev polynomials. Gabor schemes have been used in a similar manner in [15] to approximate the frequency response.

For all those methods, the need of *a priori* information can lead to issues if the provided data are not relevant. For example, the distance to the first echo has to be known in order to estimate the corresponding time delay leading to non LOS contributions. Indeed, in complex environments, with several reflections, determining the location of the element causing the first echo is a non trivial task and can lead to significant errors.

As an alternative, we propose an experimental method to correct patterns obtained in echoic, partially reflective environments. Only one set of reference measurements in an anechoic chamber is needed. Two other sets of measurements are collected in the test environment to achieve the correction. The method removes the artefacts introduced by the reflections inherent to the non-anechoic environment. Since the method is based on a substitution method, the correction can be freely adapted to fit any anechoic chamber signature and does not limit the correction to free space pattern. The method relies on an angular transfer function deconvolution from echoic patterns, originally proposed in [16] and validated numerically in theoretical settings, for fully anechoic environments. Here, we are extending the method to non-fully anechoic environments and implementing it experimentally. This paper is thus the first experimental validation of the theoretical method proposed in [16]. It demonstrates that the method is viable as a practical echo-removing solution, albeit with some limitations, which

M. Spirlet is a PhD student with the Montefiore Institute, Department of Electrical and Computer Engineering, University Of Liège, Belgium, e-mail: maxime.spirlet@ulg.ac.be

C. Geuzaine and V. Beauvois are with the University of Liège.

are carefully analysed through multiple experiments.

The paper is organized as follows. In section II, the principles of the angular deconvolution method are presented. Section III describes the practical aspects of the method used during the experimental tests. Some validation and uncertainty results are given in section IV. Sections V to VII are dedicated to experimental and parametric test cases. We draw some conclusions in section VIII.

II. Angular Deconvolution Principles

The principles presented below are valid to reconstruct antenna patterns in a given horizontal plane. The 3D pattern reconstruction is not addressed here, but the method could nevertheless be extended to obtain such patterns. Considering an Antenna Under Test (AUT) in Free Space (FSP), the measured complex pattern P_{AUT}^{FSP} at a fixed frequency f_0 is identical to the exact pattern $P_{AUT}(\theta)$, where θ is the azimuthal direction arround the antenna fixed axis of rotation in the considered plane. Indeed, the true pattern is simply convolved with an azimuthal impulse, $H^{FSP}(\theta) = \delta(\theta)$, since in free-space nothing distorts the antenna pattern:

$$P_{AUT}^{FSP}(\theta) = P_{AUT}(\theta) \star H^{FSP}(\theta) = P_{AUT}(\theta). \quad (1)$$

Achieving the same measurement in the test echoic environment (TEST) will lead to a new distorted pattern P_{AUT}^{TEST}, which will be the ideal pattern P_{AUT} convolved by a non trivial function, depending on the environment $H^{TEST}(\theta)$:

$$P_{AUT}^{TEST}(\theta) = P_{AUT}(\theta) \star H^{TEST}(\theta). \quad (2)$$

If the antenna pattern in free space P_{REF} is known for a given reference antenna, then, the reponse of the environment can be extracted from (1) by using a DFT on the azimuthal sequences:

$$H^{TEST}(\theta) = \mathcal{F}_\vartheta^{-1}\left(\frac{\mathcal{F}_\theta\left(P_{REF}^{TEST}\right)}{\mathcal{F}_\theta\left(P_{REF}\right)}\right), \quad (3)$$

where $\mathcal{F}_\theta(\cdot)$ and $\mathcal{F}_\vartheta^{-1}(\cdot)$ denote the discrete and the inverse discrete Fourier transform in the angular domain and the division is performed mode by mode (i.e. element-wise in the DFT vectors).

Now, using the AUT from which the antenna pattern has to be estimated, and considering that the environment remains constant, the response H^{TEST} is also nearly constant (neglecting the second order reflections between the antenna and the environment). We thus have:

$$P_{AUT}(\theta) = \mathcal{F}_\vartheta^{-1}\left(\frac{\mathcal{F}_\theta\left(P_{AUT}^{TEST}\right)}{\mathcal{F}_\theta\left(H^{TEST}\right)}\right) \quad (4)$$

$$= \mathcal{F}_\vartheta^{-1}\left(\frac{\mathcal{F}_\theta\left(P_{AUT}^{TEST}\right)\mathcal{F}_\theta\left(P_{REF}\right)}{\mathcal{F}_\theta\left(P_{REF}^{TEST}\right)}\right). \quad (5)$$

For (5) to make sense, $\mathcal{F}_\theta\left(P_{REF}^{TEST}\right)$ should of course not have any zero mode. This can be ensured by using a regularized Fourier transform in which any component of $\mathcal{F}_\theta\left(P_{REF}^{TEST}\right)$ such that $\left|\mathcal{F}_\theta\left(P_{REF}^{TEST}\right)[\vartheta]\right| < \epsilon$ is replaced by ϵ (typically $\epsilon = 10^{-12}$).

Expression (5) can be extended to obtain the antenna pattern P_{AUT}^{REF} in a non free space reference environment by convolving each side of (4) by the response of this reference environment H^{REF}:

$$P_{AUT} \star H^{REF} = \mathcal{F}_\vartheta^{-1}\left(\frac{\mathcal{F}_\theta\left(P_{AUT}^{TEST}\right)}{\mathcal{F}_\theta\left(H^{TEST}\right)}\right) \star H^{REF}, \quad (6)$$

yielding:

$$P_{AUT}^{REF}(\theta) = \mathcal{F}_\vartheta^{-1}\left(\mathcal{F}_\theta\left(P_{AUT}^{TEST}\right)\frac{\mathcal{F}_\theta\left(H^{REF}\right)}{\mathcal{F}_\theta\left(H^{TEST}\right)}\right) \quad (7)$$

$$= \mathcal{F}_\vartheta^{-1}\left(\mathcal{F}_\theta\left(P_{AUT}^{TEST}\right)\frac{\mathcal{F}_\theta\left(H^{REF}P_{REF}\right)}{\mathcal{F}_\theta\left(H^{TEST}P_{REF}\right)}\right) \quad (8)$$

$$= \mathcal{F}_\vartheta^{-1}\left(\frac{\mathcal{F}_\theta\left(P_{AUT}^{TEST}\right)\mathcal{F}_\theta\left(P_{REF}^{REF}\right)}{\mathcal{F}_\theta\left(P_{REF}^{TEST}\right)}\right). \quad (9)$$

The constructed patterns estimated in free-space (5) or in an arbitrary environment (9) are computed in the same way. The only difference resides in the reference antenna measurement, that will be achieved either in free-space or in any other environment (e.g. semi or full anechoic chamber).

III. Experimental Angular Deconvolution Method

Practically, the method requires two steps of measurements in the test environment plus one step in the reference environment. The measurement setup remains the same for each step. Using a Vector Network Analyzer (VNA), the complex transmission coefficient S_{21} between a fixed emission antenna and a rotating antenna (reference or test) is collected along the rotation angles $\theta = n\Delta\theta,\ n = \{0, 1, ..., N-1\}$ (see Fig. 1). So, this is not the pattern of the AUT itself that will be measured, but the transmission coefficient between the fixed antenna and the AUT. To guarantee a valid reconstructed pattern, using the same fixed antenna during the whole process is mandatory since its pattern will be part of the estimated environmental response. The reconstructed pattern will be the one in the horizontal plane determined by the height of the fixed emission antenna. The height position of the two successive rotating antennas should be the same, but does not necessarily need to be the same as the fixed antenna. Moreover, it is suitable to respect the far-field condition to reduce the second order reflections between the two antennas, thus enforcing the angular environment response invariance. The working frequency f_0 remains unchanged for all measurements, but a frequency sweep can also be applied.

The first two steps are performed using a reference antenna, for which both angular patterns (test and reference environments) can be obtained. These two sets of N data will be used to estimate the transfer function between the test and the reference environments. The last step will collect the measurements in the test environment for the test pattern from the AUT to be corrected.

We have thus obtained three sets of N data:

1) $S_{REF}^{REF}(f{=}f_0, \theta{=}n\Delta\theta)$: the reference pattern in the reference environment,

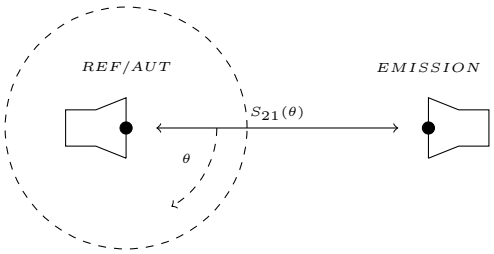

Fig. 1. Deconvolution pattern principle in an arbitrary environment.

2) $S_{REF}^{TEST}(f{=}f_0, \theta{=}n\Delta\theta)$: the reference pattern in the test environment,
3) $S_{AUT}^{TEST}(f{=}f_0, \theta{=}n\Delta\theta)$: the test pattern in the test environment (to be corrected).

To extract an angular transfer function between the environments and deconvolve it from the AUT pattern, data are processed as follows:

1) $\hat{H}_{REF}^{TEST}(f,\vartheta) = \frac{\mathcal{F}(S_{REF}^{TEST})}{\mathcal{F}(S_{REF}^{REF})}$,
2) $\hat{S}_{AUT}^{TEST}(f,\vartheta) = \mathcal{F}(S_{AUT}^{TEST})$,
3) $S_{AUT}^{REF}(f,\theta) = \mathcal{F}^{-1}\left(\frac{\hat{S}_{AUT}^{TEST}}{\hat{H}_{REF}^{TEST}}\right)$.

Numerically, the DFT is performed using the Fast Fourier Transform (FFT) algorithm [17], [18]. As mentionned in section III, $\mathcal{F}_\theta\left(P_{REF}^{TEST}\right)$ should be regularized to avoid any zero mode. However, experimentally, noise inherent in measurements naturally regularizes the angular Fourier spectrum (typically with ϵ around $-70\,\mathrm{dB}$).

IV. Experimental Validation and Uncertainty

Since the method relies on the environment transfer function invariance H^{TEST}, the simplest ideal and non trivial validation case can be achieved by using the same antenna as reference (REF) antenna and as test antenna (AUT) to prevent any unintended geometrical change. Moreover, the uncertainty of the method has been investigated through repetitive experimental tests. The goal of these measurements is to estimate the variability in the quality of reconstructed patterns. As the method had previously only been investigated numerically [16], there was no idea of the behavior of the method with respect to experimental data, i.e. data flawed due to noise and practical implementations.

The test setup is given in Fig. 2. An ultra-log antenna was used for emission. A single double ridged horn antenna has been used both for the reference antenna and for the AUT, placed at $d = 300\,\mathrm{cm}$ from the fixed antenna. The step of rotation angle was set to $\Delta\theta = 2°$. All the tests were performed in the Semi Anechoic Chamber (SAC) from the University of Liège. The chamber has been opened only once during the whole test to remove the metal plate used to reproduce an echoic environment. This metal plate was placed at $s = 200\,\mathrm{cm}$ and had a vertical surface of $1.0\,\mathrm{m}^2$.

Theoretically, it is expected to obtain a perfect reconstruction since both antennas are the same ($P_{REF}^{REF}{=}P_{AUT}^{REF}$ and $P_{REF}^{TEST}{=}P_{AUT}^{TEST}$ in (9)). The measurement without the metal plate and those with the metal plate were performed 4 times. Therefore, a total of $4^3 = 64$ reconstructed patterns were

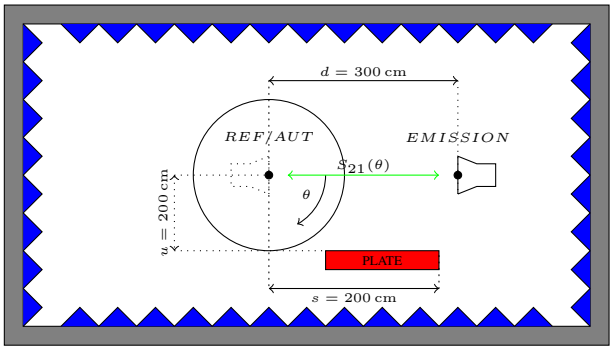

Fig. 2. Setup of the uncertainty tests.

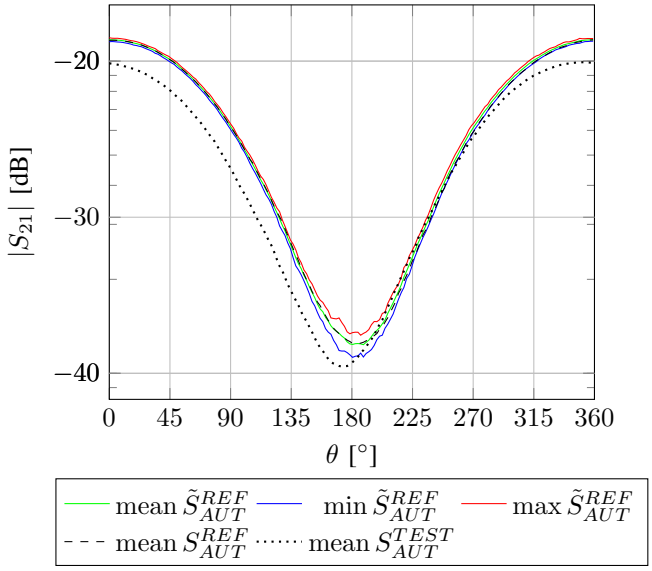

Fig. 3. Experimental deconvolution with uncertainty bounds at 200 MHz.

obtained and analyzed statistically. A frequency sweep from 200 MHz to 1000 MHz with a step of 100 MHz was also applied through the VNA.

At the end, some error bounds on the pattern reconstruction were found with respect to the azimuth angle and the frequency. The bounds were fixed to statistically encompass 99% of the samples for each considered angle. Some detailed results of the reconstructed patterns are illustrated in Figs. 3 to 5, including the minimum bound of the reconstructed pattern ($\min \tilde{S}_{AUT}^{REF}$), the maximum bound of the reconstructed pattern ($\max \tilde{S}_{AUT}^{REF}$), the mean value of the reconstructed pattern ($\mathrm{mean}\, \tilde{S}_{AUT}^{REF}$), the mean value of the measured pattern in the reference environment ($\mathrm{mean}\, S_{AUT}^{REF}$) and the mean value of the measured pattern in the test environment ($\mathrm{mean}\, S_{AUT}^{TEST}$). The choice to use mean values for reference measurements is not mandatory, but it increases graphs readability (by avoiding to draw minimum and maximum envelopes for each curves).

Globally the method is working, reconstructing a pattern close to the true pattern, with a low uncertainty. Although the artefacts caused by the environment reflections are attenuated, it is also noticeable that the quality of the reconstructed transmission coefficient ($\tilde{S}_{21}(f,\theta)$) does not remain constant, depending on the frequency and on the level of $S_{21}(\theta)$. A

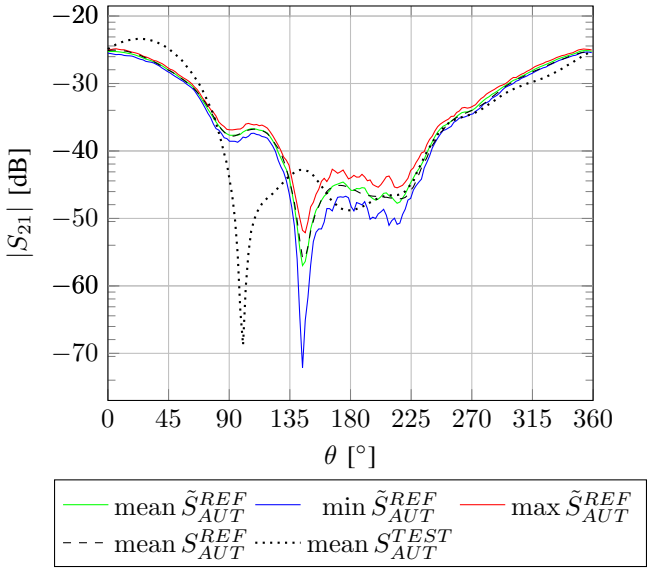

Fig. 4. Experimental deconvolution with uncertainty bounds at 500 MHz.

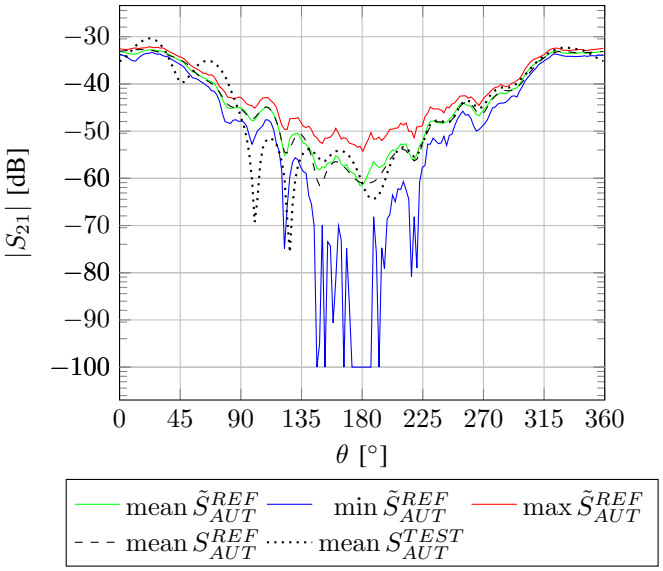

Fig. 5. Experimental deconvolution with uncertainty bounds at 1000 MHz.

deeper analysis is therefore needed to understand the quality disparity. To facilitate the analysis of the results, we introduce a composite quality index Q :

$$Q(\theta) = 1 - \frac{\operatorname{std}\tilde{S}(\theta) + \left|\operatorname{mean} S(\theta) - \operatorname{mean}\tilde{S}(\theta)\right|}{2\operatorname{mean}\tilde{S}(\theta)} \quad (10)$$

where $\operatorname{std}\cdot$ denotes the standard deviation. Here, S is S^{REF}_{AUT}, the exact measured pattern, and $\tilde{S}$ is $\tilde{S}^{REF}_{AUT}$, the reconstructed pattern. Having $Q = 1.00$ indicates the best quality of reconstruction (trueness), whereas having $Q \to 0.00$ indicates a poor reconstruction. The best indices are obtained if the standard deviation is low (good precision) and the difference between the mean value of the measured pattern and the reconstructed pattern is low (good accuracy).

The Q index is reported in Table I with respect to frequency

TABLE I
EXPERIMENTAL DECONVOLUTION UNCERTAINTY RESULTS (Q_x WHERE x IS THE FREQUENCY IN MHz).

θ	Q_{200}	Q_{300}	Q_{400}	Q_{500}	Q_{600}	Q_{700}	Q_{800}	Q_{900}	Q_{1000}
0.0°	0.99	1.00	0.99	0.99	0.97	0.98	0.98	0.97	0.99
10.0°	1.00	1.00	0.99	0.98	0.97	0.98	0.98	0.95	**0.92**
20.1°	1.00	1.00	0.99	0.98	0.97	0.97	0.99	0.98	0.98
30.1°	1.00	0.99	1.00	0.99	0.98	0.99	0.97	0.97	0.97
40.1°	1.00	1.00	0.99	0.99	0.98	0.98	0.99	0.96	0.98
50.1°	1.00	1.00	0.99	0.99	0.98	0.98	0.98	0.98	0.95
60.2°	1.00	0.99	0.99	0.99	0.98	0.97	0.97	0.96	0.97
70.2°	1.00	0.99	0.99	0.98	0.97	0.97	0.98	**0.94**	**0.94**
80.2°	1.00	0.99	0.99	0.97	0.97	0.96	0.95	**0.93**	**0.89**
90.3°	0.99	0.99	0.99	0.98	**0.94**	**0.94**	0.96	**0.88**	**0.93**
100.3°	1.00	0.98	0.98	0.98	**0.94**	**0.94**	**0.92**	**0.90**	**0.90**
110.3°	0.99	0.98	0.97	0.98	**0.91**	**0.94**	**0.93**	**0.89**	0.95
120.3°	0.99	0.98	0.98	0.98	**0.92**	**0.94**	**0.85**	**0.80**	**0.89**
130.4°	0.99	0.97	0.96	**0.94**	**0.90**	**0.85**	**0.80**	**0.80**	**0.88**
140.4°	0.98	0.97	**0.94**	**0.87**	**0.84**	**0.67**	**0.85**	**0.68**	**0.87**
150.4°	0.98	0.96	0.96	**0.89**	**0.69**	**0.71**	**0.79**	**0.74**	**0.69**
160.4°	0.98	0.96	0.97	**0.92**	**0.42**	**0.82**	**0.57**	**0.56**	**0.75**
170.5°	0.98	0.97	**0.92**	0.95	**0.84**	**0.78**	**0.83**	**0.56**	**0.79**
180.5°	0.98	0.97	**0.91**	**0.94**	**0.85**	**0.78**	**0.78**	**0.79**	**0.74**
190.5°	0.98	0.95	**0.92**	**0.91**	**0.92**	**0.77**	**0.70**	**0.83**	**0.68**
200.6°	0.98	0.96	**0.93**	**0.94**	**0.86**	**0.63**	**0.80**	**0.70**	**0.78**
210.6°	0.97	0.95	**0.93**	**0.93**	**0.92**	**0.60**	**0.36**	**0.80**	**0.83**
220.6°	0.97	0.96	0.95	**0.93**	**0.90**	**0.63**	**0.87**	**0.83**	**0.76**
230.6°	0.98	0.97	0.97	**0.92**	**0.92**	**0.76**	0.96	**0.77**	**0.86**
240.7°	0.97	0.97	0.96	0.95	0.96	**0.89**	0.96	**0.87**	**0.94**
250.7°	0.98	0.97	0.97	0.97	0.95	0.95	**0.94**	0.96	**0.92**
260.7°	0.98	0.97	0.97	0.98	**0.92**	**0.93**	0.96	**0.82**	**0.93**
270.8°	0.98	0.97	0.97	0.99	0.95	**0.92**	0.95	**0.89**	**0.90**
280.8°	0.98	0.97	0.97	0.96	**0.89**	**0.94**	0.95	0.96	0.95
290.8°	0.98	0.98	0.97	0.98	**0.94**	0.96	**0.94**	**0.93**	0.96
300.8°	0.99	0.97	0.98	0.98	0.97	0.97	0.96	0.95	**0.93**
310.9°	0.99	0.98	0.98	0.99	0.97	0.98	0.97	**0.94**	0.96
320.9°	0.99	0.98	0.99	0.98	0.98	0.98	0.98	0.97	0.97
330.9°	0.99	0.99	0.99	0.98	0.98	0.99	0.98	0.97	0.97
340.9°	0.99	0.99	0.99	0.98	0.99	0.98	0.98	0.98	0.98
351.0°	1.00	0.99	0.99	0.98	0.98	0.98	0.99	0.97	0.98

and with respect to the azimuthal angle θ. A lower bound has been chosen for Q, under which the reconstruction is considered as bad. This lower bound is fixed at $Q = 0.95$, representing a global mismatch of ≈ 1 dB. The bad Q values appear in bold face and underlined in the table.

The results tend to show that as long as $S_{21}(\theta)$ remains high, the quality of the reconstructed pattern is good. However, when the pattern contains values of $S_{21}(\theta)$ less than about -40 dB, the quality of the reconstructed patterns can dramatically decrease locally. This was expected, since the VNA measuring low amplitudes of S_{21} comes closer to the noise level, increasing the uncertainty on the collected measurements. But as long as the main beam of the pattern is considered, results remain acceptable according to the fixed criterion ($Q \geq 0.95$).

The experimental viability of the method being thus established, the following sections expose several tests cases, being more and more realistic to meet practical situations. Table II summarizes the different proposed test cases in sections V to VII.

V. EXPERIMENTAL TEST CASES IN SEMI-ANECHOIC ENVIRONMENT

Using two test cases, we have tested the complete method using the SAC as reference environment. A simple echoic test environment was simulated by introducing a metal plate (1 m × 1 m) in the SAC, as described in Fig. 6 for the first test case and Fig. 7 for the second one. For each case, the three needed angular data sets were obtained, plus the true reference set for comparison.

TABLE II
SUMMARY OF THE PROPOSED TEST CASES.

Section	Test cases	Antenna	Reference Setup	Results
Section V	1	log-periodic	Fig. 6 (Fig. 8)	Fig. 9
	2	yagi-uda	Fig. 7	Fig. 10
Section VI	Parametric d	log-periodic	Fig. 6	Fig. 11
	Parametric d	yagi-uda	Fig. 6	Fig. 12
	Parametric s	log-periodic	Fig. 6	Fig. 13
	Parametric s	yagi-uda	Fig. 6	Fig. 14
	3	log-periodic	Fig. 7	Fig. 16
	4	yagi-uda	Fig. 7 (Fig. 15)	Fig. 17
Section VII	5	yagi-uda	Fig. 7	Fig. 18
	6	yagi-uda	Fig. 7 (Fig. 19)	Fig. 20

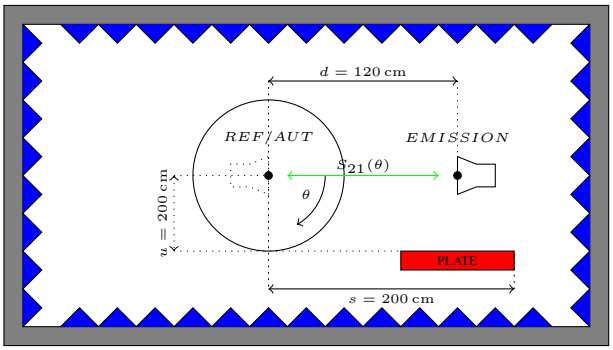

Fig. 6. Setup of the test case 1

In the first case, the distance s between the rotating antenna and the metal plate was $2.0\,\mathrm{m}$ while in the second case, the plate was placed at $t = 1.6\,\mathrm{m}$ behind the rotating antenna.

For both tests cases, the distance between the rotating antenna and the static antenna was fixed to $d = 1.20\,\mathrm{m}$. The working frequency was set to $1.0\,\mathrm{GHz}$. The emission antenna was a log-periodic antenna in the first case, and was a yagi-uda antenna in the second case. The rotating antennas were two different double-ridged horn antennas (Rohde & Schwarz HL907 and Schwarzbeck BBHA-9120-AS). A Rohde & Schwarz ZVA24 VNA driven by a computer sofware was used for data acquisition via GPIB. The same software was also driving the turntable from the SAC to incrementally rotate the antennas ($\Delta\theta = 2°$). Fig. 8 depicts the real experimental setup in the echoic configuration, with the metal plate simulating a simple echoic environment.

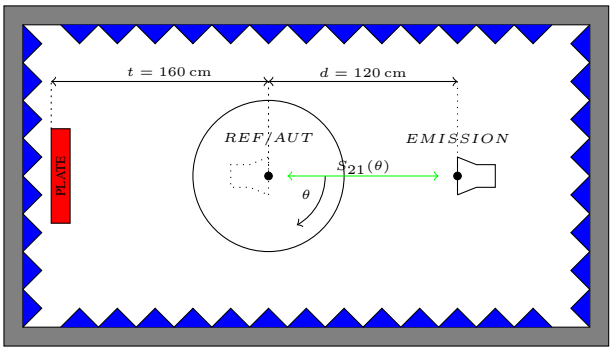

Fig. 7. Setup of the test case 2.

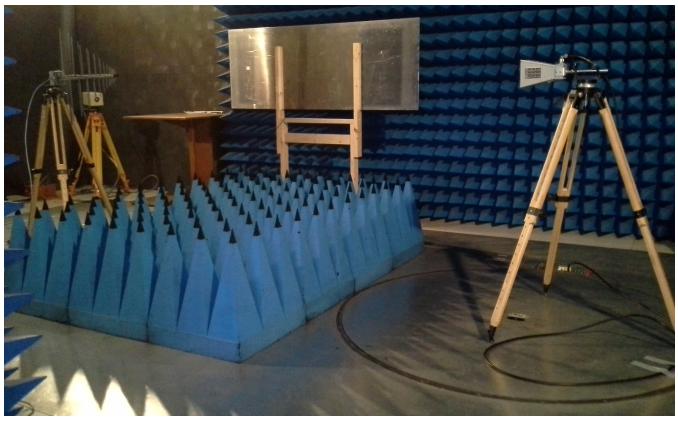

Fig. 8. Experimental deconvolution setup for test case 1.

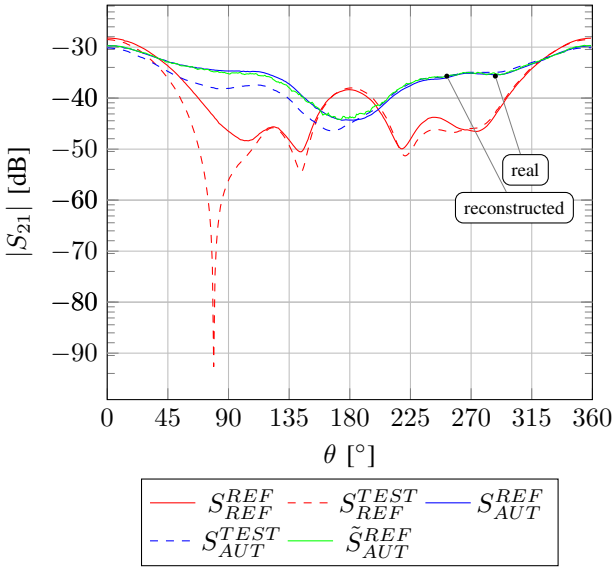

Fig. 9. Experimental deconvolution results for test case 1.

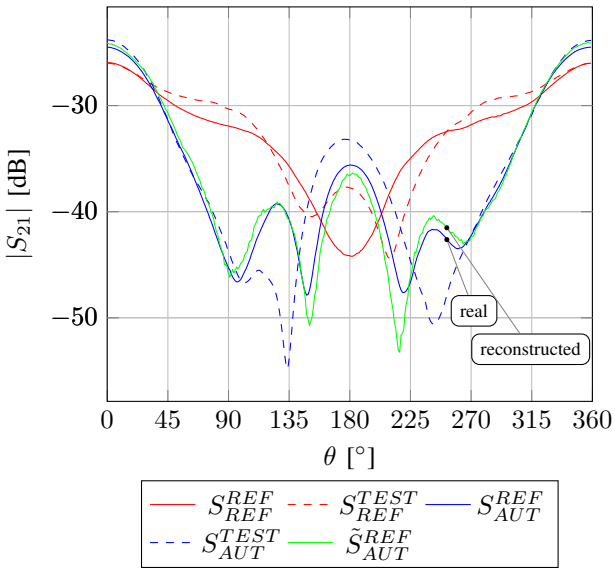

Fig. 10. Experimental deconvolution results for test case 2.

The three sets of measured data S_{REF}^{REF}, S_{REF}^{TEST}, S_{AUT}^{TEST}, the corrected pattern $\tilde{S}_{AUT}^{REF}$ and the true pattern S_{AUT}^{REF} of the AUT are shown in Fig. 9 for the first test case, and in Fig. 10 for the second test case. Comparing the reconstructed pattern $\tilde{S}_{AUT}^{REF}$ to S_{AUT}^{REF} on Fig. 9, it appears that the matching is excellent. The reconstructed pattern follows less accurately the true one in the second test case, as seen in Fig. 10. A possible explanation may come from the increase of the uncertainty for lower amplitudes of the transmission coefficient, which are most present in the second test case than in the first test case.

Those results show that in both cases, by applying the deconvolution method, the echoic artefacts are suppressed or highly attenuated, and the reconstructed patterns are getting closer to the true patterns.

VI. Experimental Parametric Test Cases

Based on the results from section V, the behavior of the method according to the position of the reflective elements and the antennas is not obvious. In order to establish some rules to obtain accurate reconstructed patterns, we have completed parametric test cases, varying the distance d between the fixed antenna and the rotating antenna on one hand (see Fig. 6), and on the other hand, varying the distance s between the rotating antenna and the metal plate (see Fig. 6). The tests have been achieved using either a low directive antenna (log-periodic) or a high directive antenna (yagi-uda) as fixed antenna, to compare the efficiency of the method regarding the emission antenna type.

In all tests, we have considered the error between the real pattern and the reconstructed pattern according to the following formula:

$$E_S = \sqrt{\left| \frac{\sum_{i=0}^{N-1} \left(\left| S_{AUT}^{REF}(\theta_i) \right| - \left| \tilde{S}_{AUT}^{REF}(\theta_i) \right| \right)^2}{\sum_{i=0}^{N-1} \left| S_{AUT}^{REF}(\theta_i) \right|^2} \right|}. \quad (11)$$

The maximum error allowed has been estimated by averaging the errors obtained by (11) on the 64 results from the validation and uncertainty tests from section IV for the frequency of 300.0 MHz, corresponding to the global worse satifactory quality pattern encountered, and has been fixed to 5.6 % (−25 dB) (considering a confidence interval of 99 %).

To be able to compute the errors, we measured, for each antenna, the pattern in the reference environment and in the test environment. As a result we can use both antennas for reference, reconstructing the pattern of the other antenna. In the following results, "Antenna A" denotes the error on the reconstruction of the pattern for the first antenna with the second antenna as reference, whereas "Antenna B" denotes the error on the reconstruction of the pattern for the second antenna, using the first antenna as reference.

A. Varying the distance d between the two antennas

The same configuration setup as for the first test case (Fig. 6) was used, but the distance d between the antennas has been changed between 120 cm and 450 cm. The error with the log-periodic emission antenna is summarized in Fig. 11, whereas the error with the yagi-uda is reported in Fig. 12.

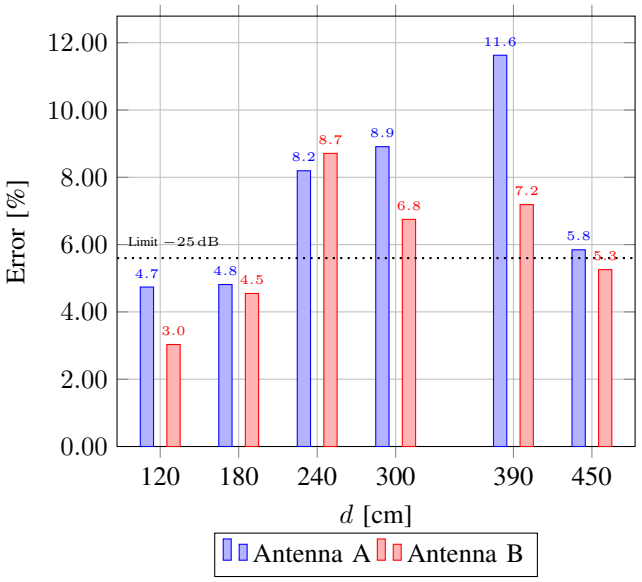

Fig. 11. Parametric results depending on d for the experimental deconvolution at 1000 MHz, using a log-periodic fixed antenna.

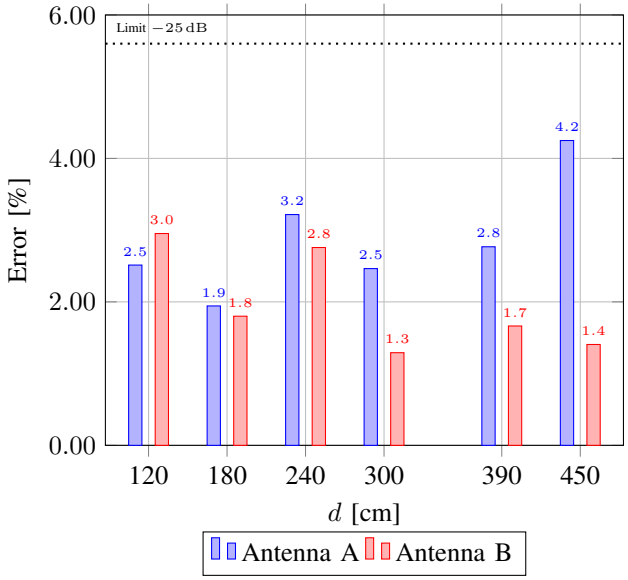

Fig. 12. Parametric results depending on d for the experimental deconvolution at 1000 MHz, using a yagi-uda fixed antenna.

Fig. 11 shows that the error is globally high for the distances between the fixed and the rotating antenna from 240 cm to 390 cm. This can be explained by the conjuction of two facts: first, in this configuration, the metal plate is postionned half way from the two antennas, and therefore the reflections are probably the most impinging on the rotating antenna, making the environment transfer function non invariant from reference antenna to AUT configuration; and second, with the increasing distance, the value of S_{21} decreases, increasing the uncertainty measurement due to noise. For the yagi-uda, a more directive antenna, the errors are given in Fig. 12. The error is fairly low with an accurate pattern reconstruction according to the fixed

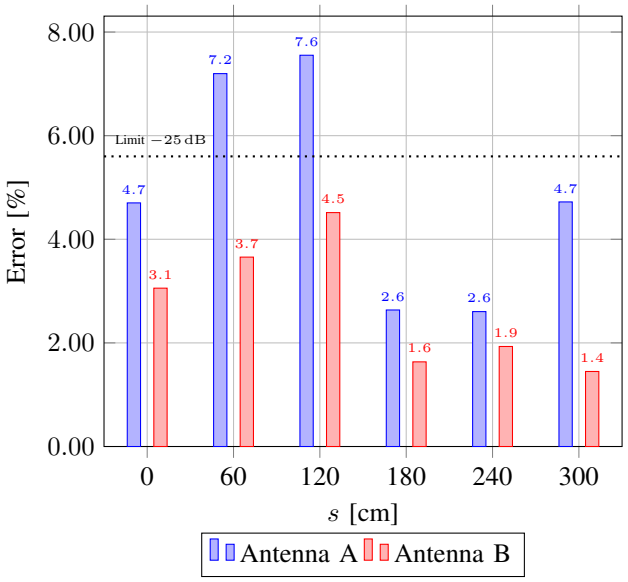

Fig. 13. Parametric results depending on s for the experimental deconvolution at 1000 MHz, using a log-periodic fixed antenna.

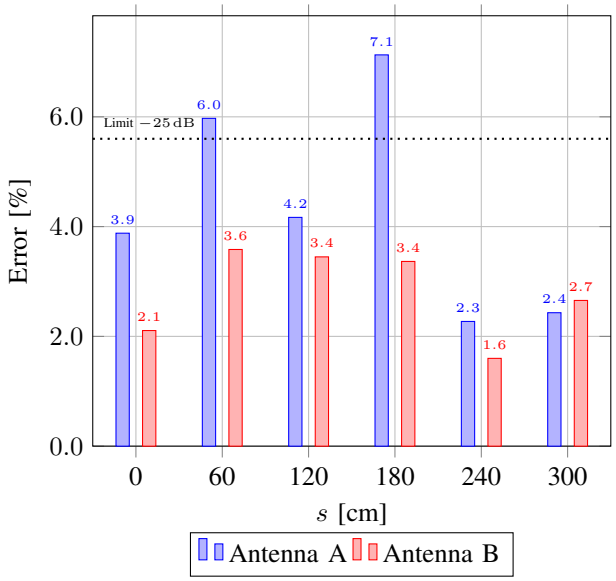

Fig. 14. Parametric results depending on s for the experimental deconvolution at 1000 MHz, using a yagi-uda fixed antenna.

criterion. In this case, the method brings a good suppression of the reflection caused by the metal plate, which would mean that the increased directivity of the emission antenna lowers the second order reflections that deteriorates the environment transfer function invariance.

B. Varying the distance s between the rotating antenna and the metal plate

The same configuration setup as for the second test case (Fig. 7) was used, but the distance s between the rotating antenna and the metal plate has been changed from 0 cm to 300 cm. The error with the log-periodic emission antenna is summarized in Fig. 13, whereas the error with the yagi-uda antenna is reported in Fig. 14. It appears that the error highly depends on the screen location, both for directive and non directive antennas. In average, the errors are almost the same for the two kinds of antennas (3.80 % and 3.56 %) with a slight advantage for directive antenna, moreover it has lower standard deviation than the less directive one (1.62 % and 2.04 %).

Accordingly, the results from the two parametric test cases tend to show that using a directive antenna for the emission antenna reduces the reconstruction errors and increases the method robustness. But the nature of the reflections has also a *predominant* impact on the quality of the reconstructed pattern, remaining difficult to predict. In order to assess this hypothesis, two more complex test cases were evaluated. The following test cases rely on a similar setup to the second test case (see Fig. 7), but the echoic environment has been complexified by introducing two additionnal metal plates, as shown in Fig. 15.

The results of test case 3, with the log-periodic antenna for emission, are shown in Fig. 16 and those for the test case 4, with the more directive antenna, yagi-uda, are shown in Fig. 17.

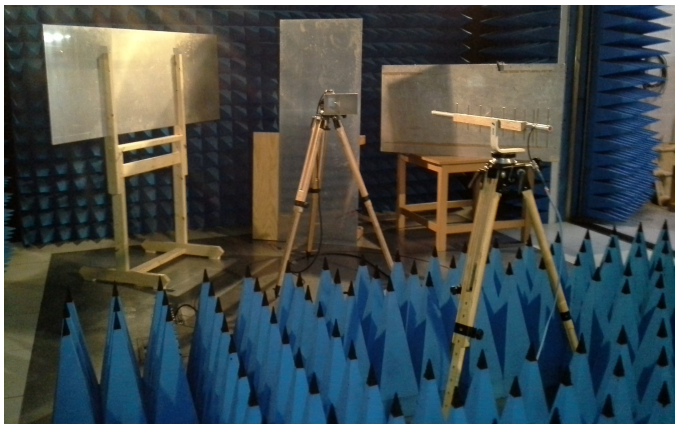

Fig. 15. Experimental deconvolution setup for test case 4.

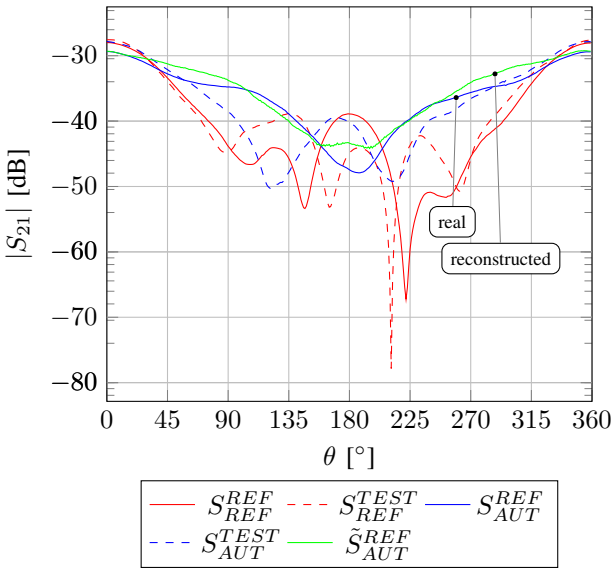

Fig. 16. Experimental deconvolution results for test case 3.

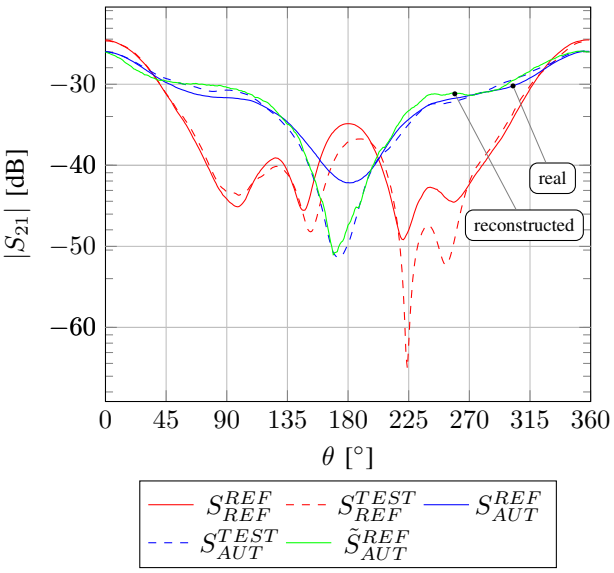

Fig. 17. Experimental deconvolution results for test case 4.

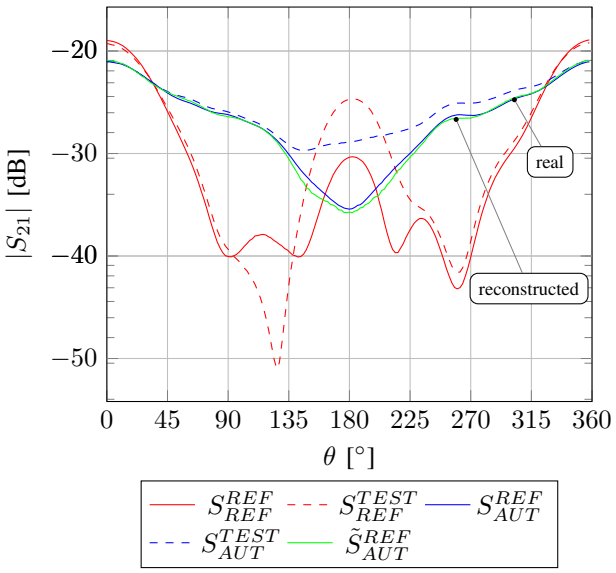

Fig. 18. Experimental deconvolution results for test case 5.

The reconstructed pattern have a really poor accuracy in both cases compared to our quality limit of $5.6\,\%$ (errors according to (11): $14.4\,\%$ for the log-periodic and $9.3\,\%$ for the yagi-uda). The correction has almost no effect in the case of the directionnal antenna, and few effects for the less directionnal antenna. A hypothetic cause may be the reflections between the metal plates and the rotating antenna that differ too much with the geometry of the two rotating antennas. Theoretically, the method works only if the environment does not change during the rotation of the two antennas in the test environment. Here this might not be the case anymore. However, it should be noticed that even if the method does not always produce an accurate pattern, it does not produce a worse pattern than the non-corrected echoic pattern.

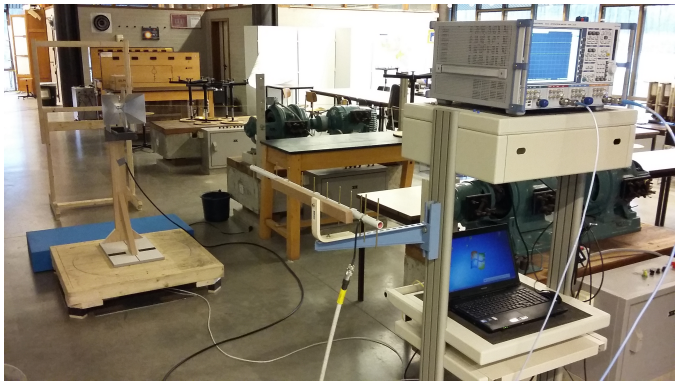

Fig. 19. Experimental deconvolution setup for test case 6.

VII. Experimental Test Cases in Realistic Environment

The angular deconvolution method has been tested experimentally in a realistic environment. The method has been applied to experimental results collected from a rather echoic complex environment, which was an electrical machines test benches laboratory. A metal plate was used to modify the echoic signature of the environment. The configuration setup was really close to the one of the test case 2 (Fig. 7). The yagi-uda antenna was used since the previous tests have shown that a directive emission antenna seems to improve the quality of the reconstructed patterns.

The objective of this test case 5 was to evaluate the behavior of the method in a complex environment, but with just a few changes between the reference and the test environment. The results of the reconstruction, and the measured data are shown in Fig. 18, and it is obvious that the reconstructed pattern $\tilde{S}_{AUT}^{REF}$ matches accurately with the measured pattern S_{AUT}^{REF}.

This final test case aims to extends the previous test case 5 in realistic environments. We used the same test environment as in test case 5, depicted in Fig. 19, but the considered reference environment was the Full Anechoic Chamber (FAC) from the "Welcome Technological Platform" at the University of Louvain-La-Neuve. To do so, we achieved the measurements of the reference antenna and AUT in the FAC in the same conditions than in the test environment. Of course, the measurement setup was moved from one environment to the other, and the greatest difficulty was to conserve all the parameters unchanged except the antennas.

The results of this test case are shown in Fig. 20. The error between the true measured pattern of the AUT in the FAC is quite close to the reconstructed pattern. It is a bit worse than for test case 5, but it should be reminded that the whole setup was moved from one place to another and, despite the fact that the different elements of the setup were displaced with the greatest care, some errors have unmistakably been introduced.

In practice these last two test cases demonstrate that the proposed angular deconvolution approach could be a promising method to retrieve radiation patterns for in-situ measurements.

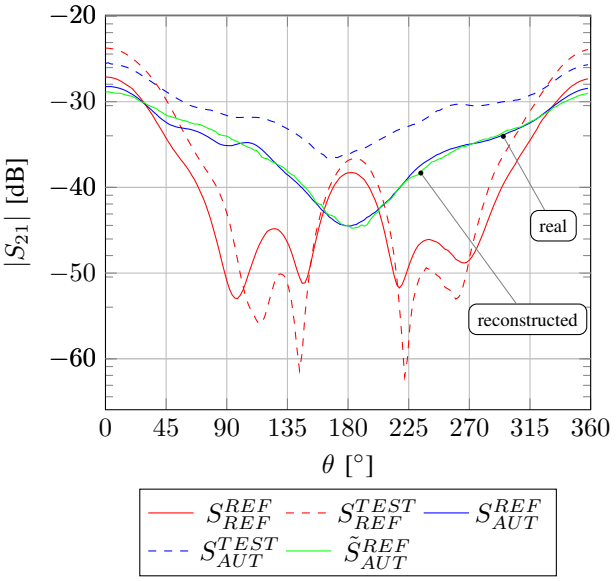

Fig. 20. Experimental deconvolution results for test case 6.

VIII. Conclusions

An angular deconvolution method has been applied experimentally. The method estimates a response between two environments and deconvolve it from a flawed pattern. To our best knowledge, these are the first experimental results based on this method.

The method has been first validated through simple experimental test cases. The results have shown that the method could be used with experimental data to reconstruct accurate patterns. However, the accuracy depends on the measured amplitude levels, given that low amplitudes are more prone to be noise sensitive than higher ones. But considering the higher amplitudes from the main beams of the patterns, the quality of the reconstruction is generally satisfactory for estimation purposes.

Some parametric test cases have been performed to identify the key parameters to obtain quality pattern reconstructions. Those results tend to show that using a directive emission antenna reduces the reconstruction errors and increases the method robustness. But the most important factor seems to be the reflections themselves. Their way of interacting with the antennas can lead to significant errors of reconstruction. This is probably due to the reflections between the environment and the rotating antennas that prevents the angular environment response to be almost constant. But due to the difficulty to isolate and decorrelate that parameter from the others, we cannot reliably conclude.

Finally, more realistic test cases have been achieved. The method has provided accurate reconstruction patterns, giving a good estimation of a true pattern measured in a FAC, but with only a single set of measurement obtained in the FAC. Such an estimation method is therefore interesting to reduce the cost and the time spent to occupy dedicated test facilities.

Acknowledgment

The authors would like to thank the University of Louvain-La-Neuve (Belgium) for the availabilty of its FAC.

References

[1] I.S.O., *ISO 5725 : Accuracy (trueness and precision) of measurement methods and results*, 1994.

[2] A. E. Fridman, *The Quality of Measurements: A Metrological Reference*. New York, NY: Springer New York, 2012. [Online]. Available: http://dx.doi.org/10.1007/978-1-4614-1478-0

[3] S. G. Rabinovich, *Measurement Errors and Uncertainties: Theory and Practice*. New York, NY: Springer New York, 2005. [Online]. Available: http://dx.doi.org/10.1007/0-387-29143-1

[4] J. Black, D.N. and E. Joy, "Test zone field compensation," *Antennas and Propagation, IEEE Transactions on*, vol. 43, no. 4, pp. 362–368, Apr 1995.

[5] S. Loredo, M. Pino, F. Las-Heras, and T. Sarkar, "Echo identification and cancellation techniques for antenna measurement in non-anechoic test sites," *Antennas and Propagation Magazine, IEEE*, vol. 46, no. 1, pp. 100–107, Feb 2004.

[6] Y. Hua and T. Sarkar, "Matrix pencil method for estimating parameters of exponentially damped/undamped sinusoids in noise," *Acoustics, Speech and Signal Processing, IEEE Transactions on*, vol. 38, no. 5, pp. 814–824, May 1990.

[7] ——, "On svd for estimating generalized eigenvalues of singular matrix pencil in noise," in *Circuits and Systems, 1991., IEEE International Symposium on*, June 1991, pp. 2780–2783 vol.5.

[8] B. Fourestie, Z. Altman, and M. Kanda, "Anechoic chamber evaluation using the matrix pencil method," *Electromagnetic Compatibility, IEEE Transactions on*, vol. 41, no. 3, pp. 169–174, Aug 1999.

[9] B. Fourestie, Z. Altman, J. Wiart, and A. Azoulay, "Correlate measurements at different test sites," *Antennas and Propagation, IEEE Transactions on*, vol. 47, no. 10, pp. 1569–1573, Oct 1999.

[10] B. Fourestie, Z. Altman, and M. Kanda, "Efficient detection of resonances in anechoic chambers using the matrix pencil method," *Electromagnetic Compatibility, IEEE Transactions on*, vol. 42, no. 1, pp. 1–5, Feb 2000.

[11] G. Leon Fernandez, S. Loredo, S. Zapatero, and F. Las Heras Andres, "Radiation pattern retrieval in non-anechoic chambers using the matrix pencil algorithm," *Progress In Electromagnetics Research Letters*, vol. 9, pp. 119–127, 2009. [Online]. Available: http://www.jpier.org/pierl/pier.php?paper=09051204

[12] R. Ayestaran, G. Leon, S. Loredo, J. LOPEZ-FERNANDEZ, and F. Las-Heras, "Sparse deconvolution based on regularisation for echo correction in antenna measurement," *Microwaves, Antennas Propagation, IET*, vol. 6, no. 12, pp. 1299–1305, September 2012.

[13] M. Sacchi, T. Ulrych, and C. Walker, "Interpolation and extrapolation using a high-resolution discrete fourier transform," *Signal Processing, IEEE Transactions on*, vol. 46, no. 1, pp. 31–38, Jan 1998.

[14] Z. Du, J. I. Moon, S. soo Oh, J. Koh, and T. K. Sarkar, "Generation of free space radiation patterns from non-anechoic measurements using chebyshev polynomials," *Antennas and Propagation, IEEE Transactions on*, vol. 58, no. 8, pp. 2785–2790, Aug 2010.

[15] B. Fourestie and Z. Altman, "Gabor schemes for analyzing antenna measurements," *Antennas and Propagation, IEEE Transactions on*, vol. 49, no. 9, pp. 1245–1253, Sep 2001.

[16] J. Koh, A. De, T. Sarkar, H. Moon, W. Zhao, and M. Salazar-Palma, "Free space radiation pattern reconstruction from non-anechoic measurements using an impulse response of the environment," *Antennas and Propagation, IEEE Transactions on*, vol. 60, no. 2, pp. 821–831, Feb 2012.

[17] J. W. T. James W. Cooley, "An algorithm for the machine calculation of complex fourier series," *Mathematics of Computation*, vol. 19, no. 90, pp. 297–301, 1965. [Online]. Available: http://www.jstor.org/stable/2003354

[18] M. Frigo and S. Johnson, "Fftw: an adaptive software architecture for the fft," in *Acoustics, Speech and Signal Processing, 1998. Proceedings of the 1998 IEEE International Conference on*, vol. 3, May 1998, pp. 1381–1384 vol.3.